ADVANCED FUNCTIONAL MATERIALS
www.afm-journal.de

Impact of Amorphous LiF Coating Layers on Cathode-Electrolyte Interfaces in Solid-State Batteries

*Taiping Hu, Linhan Xu, Fuzhi Dai, Guobing Zhou, Fangjia Fu, Xiaoxu Wang, Linsen Li, Xinping Ai, and Shenzhen Xu**

High interfacial resistance between electrodes and solid-state electrolyte is the major cause for the failure of all-solid-state Li-ion batteries. Spontaneous (electro)chemical reactions and poor Li-ion diffusion at the interfaces are closely related to this increased impedance. Although introducing a coating layer can mitigate interfacial reactions and structural reconstruction, it may also lead to poor Li-ion diffusion. Balancing this trade-off therefore is crucial for the design of coating layer materials. In this study, the impact of the amorphous LiF (a-LiF) coating layer on interfacial structural reconstruction and Li-ion diffusion at the $LiCoO_2$/Li_6PS_5Cl solid-state interface is explicitly elucidated via machine-learning-assisted molecular dynamics (MD) simulations. It is found that the a-LiF can effectively protect the P-S tetrahedron local structures in Li_6PS_5Cl but cannot suppress the formation of side product S_2 dimers. It is further discovered that once the a-LiF coating exceeds a certain critical thickness, emergence of ordered local structures will inhibit Li-ion diffusion. The simulations propose that the optimal thickness of the coating layer is around 1 nm. Overall, the work provides a microscopic understanding for effects of the a-LiF coating layer on the structural and kinetic properties of cathode-solid electrolyte interfaces and can guide the design of interfacial coating materials for solid-state batteries.

1. Introduction

The rapid development and growing demand for high-performance energy storage devices have spurred extensive research of all-solid-state Li-ion batteries (ASSLBs).[1–4] ASSLBs offer several advantages over conventional liquid-electrolyte-based counterparts, including higher energy density and improved safety.[5] Considerable efforts have been devoted in developing solid-state electrolytes (SEs) with high ionic conductivities. In particular, various types of Li ion conductors have been demonstrated to exhibit exceptionally high ionic conductivities ($> 10\ mS\ cm^{-1}$) at room temperature, comparable to those of liquid electrolytes.[6–17] Nevertheless, interfacial issues have emerged as the primary factors hindering the electrochemical performance of ASSLBs, limiting their potential for further commercial applications.[18]

The interfacial issues mainly reflect the increased interfacial impedance in the

T. Hu, S. Xu
Beijing Key Laboratory of Theory and Technology for Advanced Battery Materials
School of Materials Science and Engineering
Peking University
Beijing 100871, P. R. China
E-mail: xushenzhen@pku.edu.cn

T. Hu, F. Dai, F. Fu, X. Wang, S. Xu
AI for Science Institute
Beijing 100084, P. R. China

L. Xu
Liaoning Academy of Materials
Shenyang 110167, P. R. China

F. Dai, X. Wang
DP Technology
Beijing 100080, P. R. China

G. Zhou
Institute of Advanced Materials
Jiangxi Normal University
Nanchang 330022, P. R. China

F. Fu
School of Mathematical Sciences
Peking University
Beijing 100871, P. R. China

L. Li
Department of Chemical Engineering
Shanghai Electrochemical Energy Device Research Center (SEED)
School of Chemistry and Chemical Engineering
Frontiers Science Center for Transformative Molecules
Shanghai Jiao Tong University
Shanghai 200240, P. R. China

X. Ai
College of Chemistry and Molecular Sciences
Hubei Key Laboratory of Electrochemical Power Sources
Wuhan University
Wuhan 430072, P. R. China

The ORCID identification number(s) for the author(s) of this article can be found under https://doi.org/10.1002/adfm.202402993

DOI: 10.1002/adfm.202402993

electrochemical cycle. Possible reasons for this increased resistance include interfacial reactions and reconstructions, decompositions of electrolytes, inadequate contacts between the electrode and electrolytes. Many experimental strategies have been developed to mitigate the interfacial resistance. For instance, introducing a stable coating layer on the cathode surface has proven to be effective in preventing interfacial reactions and promoting the interfacial stability. Various coatings, such as metal oxides,[19–23] phosphate- and halide-based,[24,25] have been applied to protect interfaces. A suitable coating material should follow two principles: (1) it can effectively inhibit interfacial reactions by isolating the electrode and electrolyte; (2) it possesses a good ionic conductivity. In reality, it is difficult to achieve promising performance for both of these two aspects. For example, some binary coatings, such as Al_2O_3 and SiO_2, are chemically stable, but lack ionic diffusivities.[26,27] Therefore, balancing the aforementioned stability and ionic transport is crucial for the design of coating layer materials.

Over the past few years, thermodynamic analysis based on density functional theory (DFT) calculations have been widely used to unravel interfacial properties, such as the electrochemical stability, potential reaction products, the impact of the coating on the space charge layer formation, and so on.[28–34] Furthermore, DFT-based *ab-initio* molecular dynamic (AIMD) simulations have also been applied to reveal reaction dynamics of both the cathode/SEs and Li metal anode/SEs interfaces.[29,35–37] However, substantial computational cost greatly limits the spatial and temporal scales. As a result, capturing long-time reaction dynamics and Li-ion diffusion through the reconstructed interfacial region in the presence/absence of coating materials, still remains challenging.

In this study, we use the $LiCoO_2$ (LCO) cathode and argyrodite-type electrolyte Li_6PS_5Cl (LPSCl) as a prototypical model to investigate the structural evolution of the LCO/LPSCl interface. We choose this cathode-solid electrolyte combination because (1) LCO exhibits a high energy density and dominates the 3C electronic market, thus is a good representative modeling system for cathode materials; (2) LPSCl exhibits a high ionic conductivity,[9] good cell performance[38] and stability.[39] In this work, we first employ machine-learning-assisted molecular dynamics (MD) simulations on relatively large-size LCO/LPSCl models (including several thousand atoms) to reveal the interfacial structural reconstruction and side products formation. We then further investigate the impact of the amorphous LiF (a-LiF) coating on both of the interfacial structural evolution and Li-ion diffusion. LiF is a commonly used coating material for cathode surfaces.[40–46] Moreover, a-LiF was also found in the cathode electrolyte interface (CEI).[47,48] In fact, constructing LiF-rich interphases is regarded as an effective strategy in promoting interfacial stability. Exploring effects of the a-LiF coating layer thus can deepen our understanding for its influence on solid-solid interfaces in ASSLBs. Our simulation results show that interposition of the a-LiF coating can effectively suppress the interfacial side reactions and protect the P-S tetrahedrons in LPSCl by separation between the cathode and solid electrolyte materials. While for the CEI component S_2 dimers, we find that the a-LiF coating cannot hinder their formation. We also observe that Li-ion diffusion is significantly affected by the thickness of the a-LiF coating layer. Our simulations suggest that an optimal thickness is ≈ 1 nm, at which good interfacial stability and fast Li-ion diffusion can be simultaneously ensured.

2. Results and Discussion

We first validate the accuracy of the machine-learning potential (MLP) by comparing energies and forces predicted by the DFT+U and deep potential (DP) models. We can see that the energies and forces predicted by the DP model on both the training dataset and testing dataset are in good agreement with the DFT+U results (**Figure 1b**). The total root mean square errors (RMSEs) of energies and forces on the training dataset are 1.5 meV/atom and 85.0 meV $Å^{-1}$, respectively. More importantly, similar accuracies on the testing dataset are achieved (RMSEs are 2.5 meV $atom^{-1}$ for energies and 109.7 meV $Å^{-1}$ for forces), indicating our promising DP potential model. Here, we used a converged DP model to run a 200 ps trajectory and then randomly selected 200 snapshots as the testing dataset. We can see that our DP test results are within an acceptable error range by comparing with earlier studies using MLPs.[30,49–51] Furthermore, we also performed AIMD simulations on the bare LCO/LPSCl interface and conducted the radial distribution function (RDF) analysis. Both the P-S and S-S pairs' RDF profiles obtained from the deep potential molecular dynamics (DeePMD) simulations well reproduce the results from the AIMD simulations, which demonstrates the validity of our DP model (see Figure S1, Supporting Information).

We now analyze possible interfacial reactions and the corresponding products when the cathode and solid electrolyte come into contact. Spontaneous interfacial reactions arise from the intrinsic thermodynamic instability between the cathode and solid electrolyte materials, and those reactions could be accelerated if Li vacancies are present in the system. We thus construct two types of LCO/LPSCl models, one of which contains ≈ 10% Li vacancies by randomly removing Li atoms from the LPSCl, the other model is Li-vacancy (Li_{vac}) free. Introduction of Li vacancies not only accelerates interfacial reconstructions, but also is beneficial for enhancing Li-ion diffusion.

MD simulations provide comprehensive insights into dynamic processes, enabling us to analyze the time evolution of RDFs for specific atomic pairs. This information can be used to identify potential interfacial products and qualitatively obtain timescales of the corresponding side reactions. Here, we calculate RDF curves for P-O/P-S/Co-S/S-S pairs to investigate the interfacial structural evolution in this study. The RDF analysis of P-O/P-S/Co-S pairs are related to interfacial reactions, which may involve O-S exchange and the associated P-S tetrahedron degradations. Tracking the S-S pairs helps us detect the emergence of CEI components along the interfacial structural reconstruction process.[35] Specifically, the first peak (≈ 3.3 Å) of the S-S RDF in the interfacial model without Li vacancies corresponds to the S-S distance in the P-S tetrahedrons. In contrast, the first peak (≈ 2 Å) denotes the S-S distance in the S_2 dimer when Li vacancies are present.

As seen in **Figure 2a**, upon direct contact between the cathode and solid electrolyte (i.e., no a-LiF included in the interfacial models), the P—O and Co—S bonds appear in a short timescale. This rapid process implies that the barriers for these reactions are relatively small. We estimate the free energy barriers based on RDF analysis according to the formula $V(r) = -k_B T \ln(g(r))$,

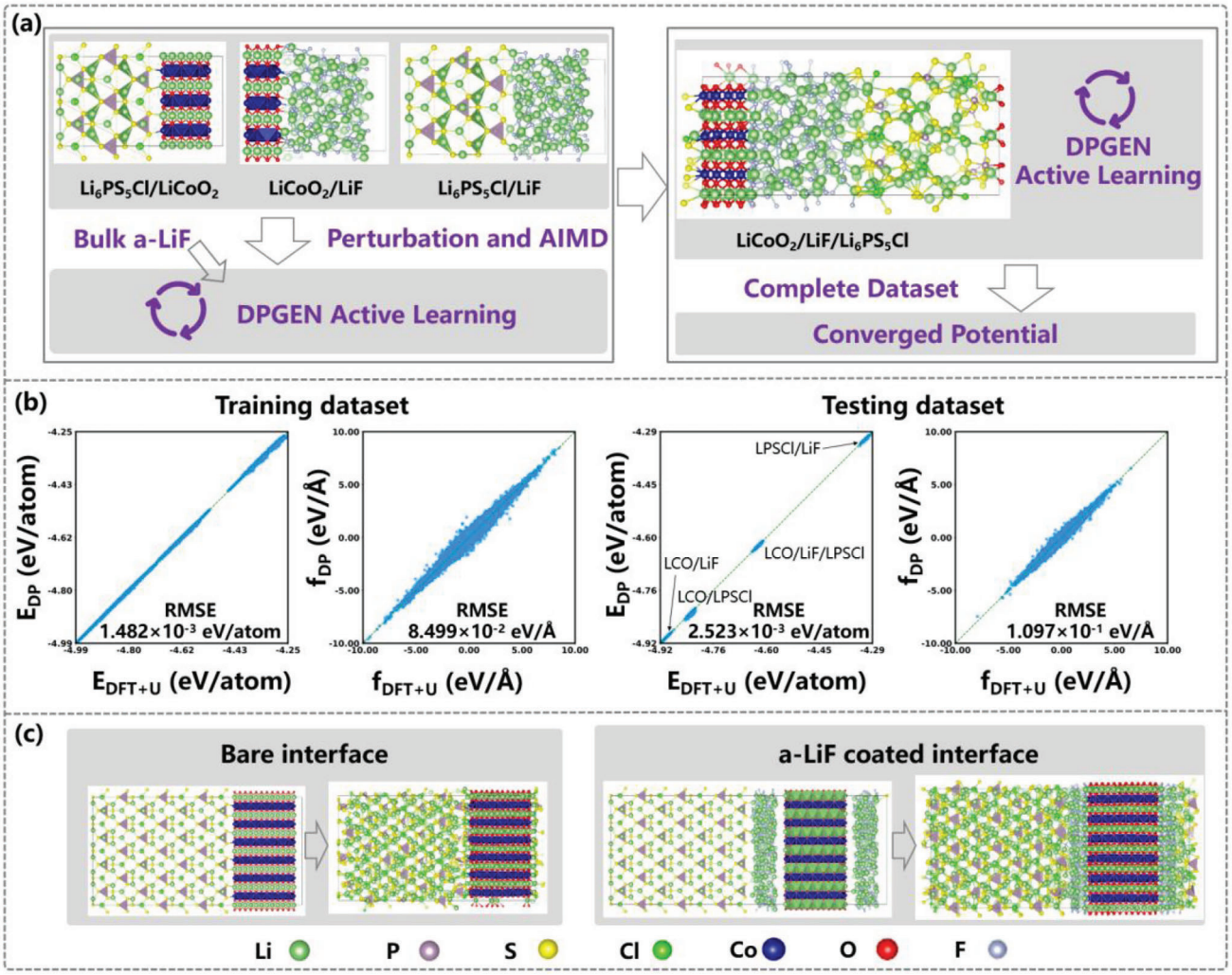

Figure 1. a) Workflow of the dataset generation. b) Comparisons of energies and forces obtained by the DP and DFT+U models on the training dataset and testing dataset. c) Atomic structures of the bare LCO/LPSCl and the a-LiF coated interfaces.

where k_B is Boltzmann constant, T is the temperature, and $g(r)$ is the RDF.[52,53] Calculated barriers are 0.09 eV for the Co—S bond formation and 0.25 eV for the P—S bond breaking. Such small barriers are consistent with our MD results. The P—O bonds formation can be attributed to the S-O exchange at the interface, as reported in previous studies.[29,35] In addition, the S-O exchange can also lead to the Co—S bond formation at the interface. As expected, these interfacial side reactions are more active in the system with Li_{vac} presence, which are reflected by the smaller/higher values of the P-S/Co-S RDF peaks. We note that, a smaller value of the P-S peak indicates some P-S tetrahedrons in the original perfect LPSCl lattice disappear due to the interfacial side reactions, thus lowering the P-S peak value in the RDF profile. Moreover, P—O bonds emerge faster in the system with Li_{vac} present (compared to the case without Li_{vac}, shown by the P-O RDF panels in Figure 2a), resulting from more active interfacial reactions induced by the Li vacancies. Tateyama et al[31] reported that configurations with cation exchanges (such as Co-P and Co-Li exchanges) are energetically favorable by combining DFT calculations with a global particle swarm optimization method. Here, we note that this method only searches thermodynamically stable configurations and cannot capture dynamics processes. We realize that the earlier reported cation-exchange products are not observed in our dynamic trajectories. A possible explanation for this discrepancy is that cation exchanges may require overcoming high-barrier transition states, it is still uncertain whether the occurrence of Co-P and Co-Li exchanges is kinetically plausible.

Our results also indicate that the interfacial reactions could induce formation of a CEI component – S_2 dimers. Here we do not mean that other side products are not components of the CEI. To maintain consistency with earlier studies, we just consider the S_2 dimer as one possible component of the CEI layer.[18,54] Our dynamic simulations show that the S_2 dimers are observed only in the system with Li vacancies (refer to the S-S panels in Figure 2a). This is because the presence of Li vacancies leads to declining interfacial stability, which facilitates the formation of CEI products.

Next, we evaluate the impact of a-LiF coating layers on the interfacial structural evolution (see **Figure 3**a). We observe that as the LiF coating layer (intercalated between LCO and LPSCl) becomes thicker, the peak values of the P-S RDF curves increase

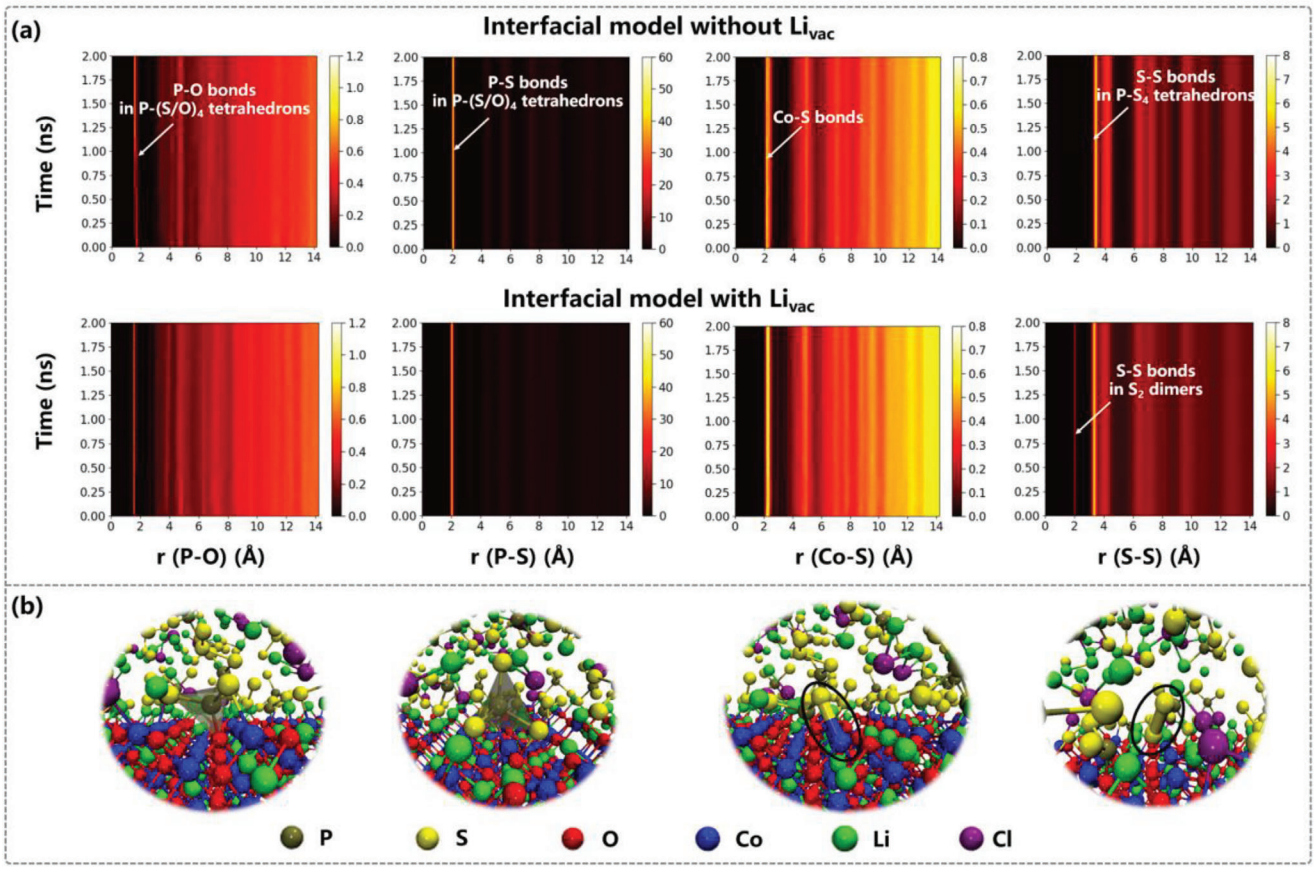

Figure 2. a) Time evolutions of specific atomic pairs' RDF profiles in the absence of Li vacancies (upper) and in the presence of Li vacancies (bottom). b) Representative morphologies for the products induced by the interfacial side reactions, corresponding to the atomic pairs in panel (a). Please note that the a-LiF coating layer is absent in all the cases presented in this figure.

(see Figure 3b), indicating that the LiF coating layer can effectively protect the P-S tetrahedrons and thus suppress the interfacial reactions. Similar phenomena can also be observed from the trend of the S-S RDF curves' variation with respect to the coating thickness (see Figure 3c). We note again that the first peak of the S-S RDF in the cases without Li_{vac} corresponds to the S-S distance in P-S tetrahedrons in a perfect LPSCl lattice (as explained above). The enhanced trend of S-S RDF peaks with respect to increasing the a-LiF thickness reflects the maintenance of more P-S tetrahedrons. The positive effect of the a-LiF coating layer on interfacial reactions thus is suppressing the unfavored S-O exchange and thereby protecting the P-S tetrahedrons in the solid electrolyte LPSCl.

We further analyze the impact of the a-LiF coating layer on the formation of CEI components. The S_2 dimers, characterized by the peak of S-S RDF in the interfacial models with Li vacancies in LPSCl (the peak position at 2 Å), still remain in systems with different a-LiF coating layer thicknesses (shown in Figure S2, Supporting Information). This indicates that although the a-LiF coating could suppress solid-solid interfacial reactions, it cannot hinder the S_2 dimer formation, which might be originated from the intrinsic instability in the LPSCl with Li vacancies present.

In addition to the coating layer's impact on the interfacial structural evolvement, Li-ion diffusion may be influenced by the coating material as well. We thus investigate the Li transport property through the a-LiF coating layer in this section. Once including a nanometer-scale coating layer in our models, direct simulations of Li-ion diffusion from LCO all the way to the solid electrolyte LPSCl require an unaffordable computational time. We instead calculate the Li-ion diffusivity in the a-LiF region, which determines the Li-transport property of the interfacial system as Li ions have to move through the coating layer during charging/discharging cycles. We increase the modeling temperature to 500 K to expedite Li diffusion in our MD simulations. We extend the simulation time lengths to 10 ns, ensuring statistical convergence of calculated diffusivities.[50] More details about relevant diffusivity calculations can be found in earlier studies.[50,55] We note that our goal in this section is not to obtain an accurate Li diffusivity, but just to explore the qualitative trend of a-LiF material's influence on Li transport with respect to the coating layer thickness.

The calculated Li diffusivities are similar between two cases with 5 Å and 10 Å a-LiF coating layers ($\sim [0.06 \pm 0.003] \times 10^{-5}$ cm^2 s^{-1} and $[0.06 \pm 0.04] \times 10^{-5}$ cm^2 s^{-1}, **Figure** 4a), indicating an almost invariant Li transport property within this thickness range. However, when the a-LiF layer thickness increases to 20Å, we find that the effective movement of Li ions significantly decreases in the a-LiF region ($\approx [0.02 \pm 0.003] \times 10^{-5}$ cm^2 s^{-1}).

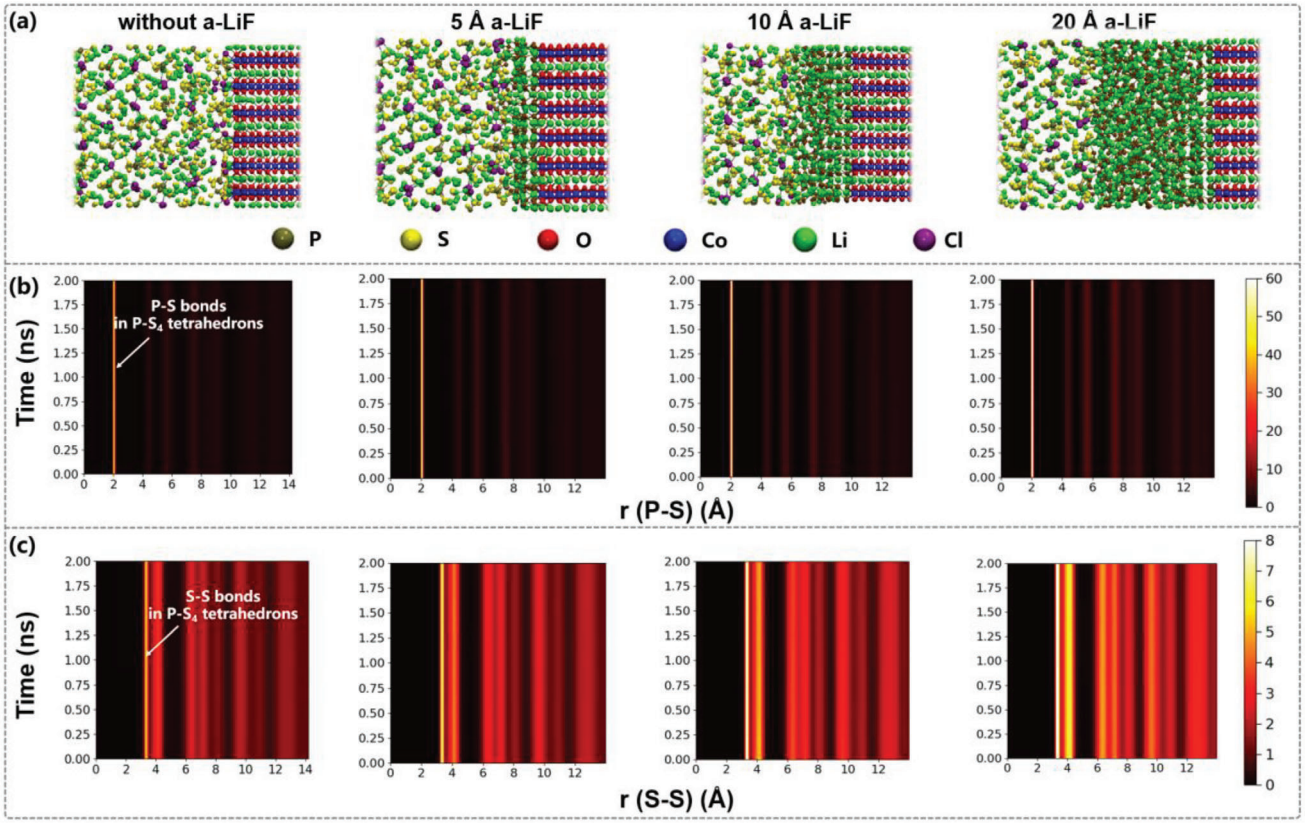

Figure 3. a) Atomic structures of the bare LCO/LPSCl and the a-LiF coated interfaces with different coating thicknesses. Time evolutions of the b) P-S and c) S-S pairs' RDF profiles in Li_{vac}-free interfacial systems. Here, the first peak's position of the S-S pair RDF corresponds to the S—S bond length in P-S tetrahedrons when no Li_{vac} is present in LPSCl, because S_2 dimers do not form under this condition.

Our dynamic trajectories reveal that the abrupt change of Li transport is caused by a local-structure transition in a-LiF when the thickness of the coating layer increases beyond a certain threshold (e.g., 20 Å in our modeling system), in which ordered regular Li-F tetrahedrons emerge in the 20 Å LiF region, and Li ions are trapped at the center of the tetrahedral cages (see Figure 4b). This local structure transition thus inhibits effective Li diffusion. In fact, similar transitions (disorder to order) in local structures were also observed in earlier large-scale simulations on the bulk phase of the CEI component a-LiF.[50] For the cathode-solid electrolyte interface model studied in this work, such a local structural transition occurs once the a-LiF coating exceeds a critical thickness, where the intrinsic bulk behaviors manifest.

The time evolutions of Li-Cl/S RDF profiles (see Figure S3, Supporting Information) also provide supportive evidences for the local-structure transition in the 20 Å thickness case, where the Li ions are from the LiF coating layer and the S/Cl ions are from the LPSCl solid electrolyte in the statistical calculations for RDFs. We can see that as the coating thickness increases, the first peaks' heights in these RDF curves gradually decrease, which can be attributed to the formation of regular Li-F tetrahedrons. The Li ions trapped at the center of Li-F tetrahedrons are unable to effectively coordinate with S/Cl ions from the LPSCl region. To further quantify the LiF structural change with respect to the coating thickness variance, we calculate the number of regular Li-F tetrahedrons (refer to SI for the definition) present in both of the 5 Å and 20 Å coating layer models (see Figure 4b). The significant increase in the number of regular Li-F tetrahedrons, from 0 to 86, suggests that the latter model exhibits a packing pattern of ordered tetrahedrons in LiF, which shut down the effective Li movement through the coating region. Consequently, we conclude that when the thickness of the a-LiF coating layer achieves a specific threshold, the emergence of ordered local structure (i.e., the regular Li-F tetrahedron) will trap Li ions and impede ionic diffusion. Our current simulation results indicate that an a-LiF coating layer of ≈ 10 Å allows effective diffusion of Li ions. Overall, our simulations point out that the design strategy of the coating layer proposed in this work can be applied to a broader class of materials that are prone to undergo phase transitions at room temperature leading to sluggish Li-ion diffusion.

3. Conclusion

In summary, we perform DeePMD simulations on large-size a-LiF coated LCO/LPSCl models to investigate impact of the coating materials on interfacial structure evolutions and Li transport properties. Our dynamic simulations reveal that the a-LiF coating layer can effectively suppress the interfacial side reactions by separating the electrode from the solid electrolyte materials. This protective effect gets strengthened with respect to the increase of the coating layer thickness. For the specific CEI component – S_2 dimers, we find that their production is more related

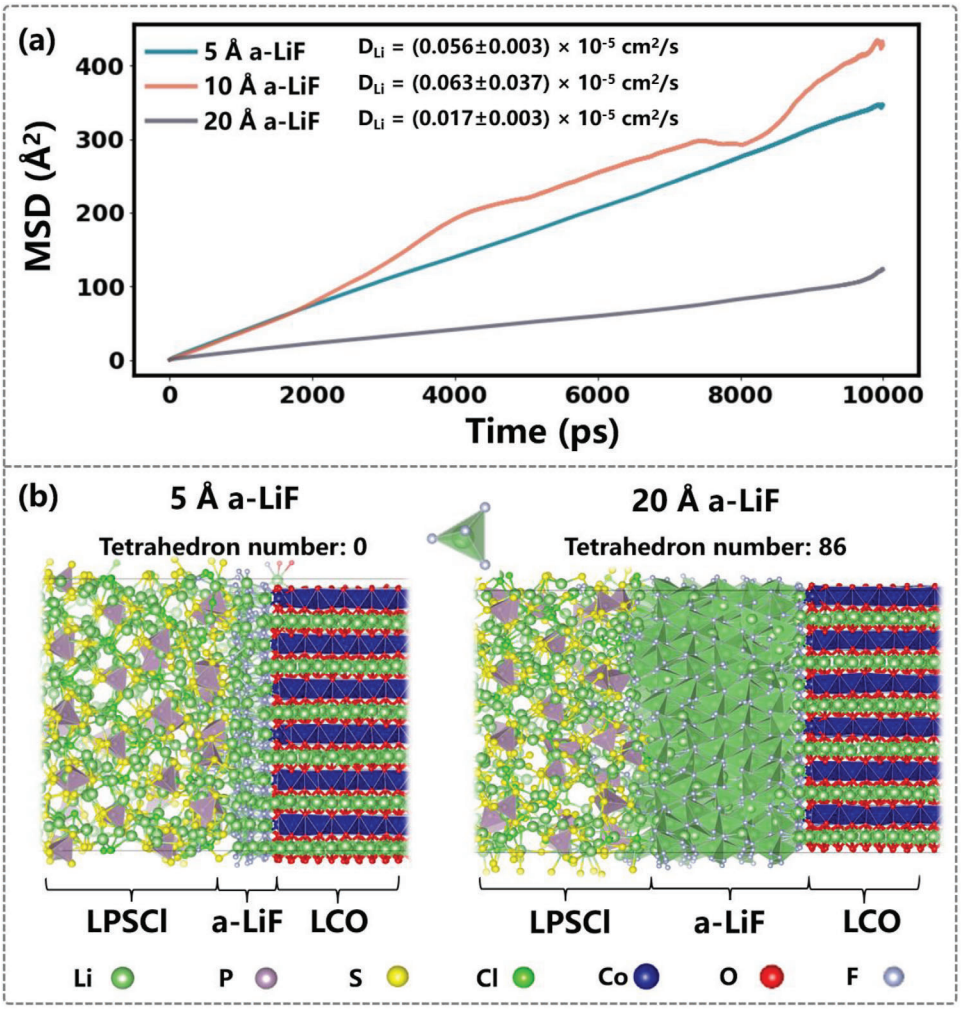

Figure 4. a) Mean square displacements (MSD) of Li ions in the a-LiF coating region with respect to simulation times in different LiF-thickness models. Calculated diffusion coefficients are presented as well. b) Atomic packing morphologies of LiF with coating layers of 5 Å and 20 Å thickness. The regular Li-F tetrahedron numbers and P-S tetrahedrons are also displayed.

to the presence of Li vacancies in the interfacial system. Regarding the impact of a-LiF coating material on Li-ion diffusion, our results reveal that once the coating layer exceeds a certain critical thickness, the emergence of ordered local structures, i.e., regular Li-F tetrahedrons, will trap Li ions and inhibit effective ionic transport. This phenomenon indicates an optimal thickness for the coating layer. Our DeePMD simulations thus provide atomic-scale mechanistic understandings for the impact of coating materials on the interfacial structure evolutions and Li-ion diffusion, and could guide the design of electrode-electrolyte interfaces in ASSLBs.

4. Experimental Section

Density Functional Theory Calculations: All DFT calculations in this work were performed using the Vienna Ab initio Simulation Package (VASP, version 5.4.4).[56,57] The projector augmented wave (PAW) potentials were employed for modeling the nuclei and the frozen-core electrons of all atoms.[58] The valence electron configurations were $1s^22s^1$ for Li, $2^{s2}2p^4$ for O, $3d^84s^1$ for Co, $3s^23p^3$ for P, $3s^23p^5$ for Cl, $3s^23p^4$ for S and $2s^22p^5$ for F. The Perdew-Burke-Ernzerhof (PBE) functional was used,[59] with the Hubbard U method[60] applied to the transition metal Co to correct so-called self-interaction errors. The U values for Co was set as 5.14 eV, consistent with previous theoretical studies.[49,61] Unless specifically explained, the only-GAMMA-centered k-point mesh and a 520 eV kinetic energy off for the plane-wave basis were used in all calculations. The energy and force (for each direction of all atoms) convergence criterions were set as 10^{-5} eV and 0.01 eV Å^{-1}, respectively. Here, non-spin-polarized DFT calculations were employed throughout the work. Since a fully lithiated LCO model was focused in this study, where the Co^{3+} spin was 0 μ_B, thus the non-spin-polarization setup is rationalized. Furthermore, the computational cost of non-magnetic DFT calculations can be significantly reduced compared to the spin-polarized cases, which improves efficiency of the force field training process and makes it practical to cover a larger configurational space of the first-principles training dataset for enhancing the accuracy of the MLP. In fact, the non-spin-polarization setups have been adopted in previous studies.[29,31–33,35]

Generation of the Dataset: The dataset used for training the deep potential model[62] was generated according to the workflow displayed in Figure 1a. It consists of two major steps: (1) DFT data generations for the LCO/LPSCl, LCO/LiF, and LPSCl/LiF interfaces; (2) DFT data generations for the a-LiF coated LCO/LPSCl interfaces (i.e., the LCO/a-LiF/LPSCl interface).

Generations for the Initial Dataset: Representative superlattice models for the LCO/LPSCl, LCO/LiF, and LPSCl/LiF interfaces were first constructed (details for the construction can be found in supporting information (SI)), as illustrated in Figure 1a. Then structural perturbations and short (100 steps) AIMD simulations were performed to generate the initial dataset. For the bulk a-LiF coating layer, the data extracted from the earlier work was just relabeled.[50] For the a-LiF coated LCO/LPSCl interface model, DPGEN[63] iterations were directly performed without preparing the initial dataset via expensive AIMD simulations.

DPGEN Iterations: The DPGEN active learning workflow[63] was employed to extend the dataset until it covers the configurational space of interest. All explorations were performed under the NPT ensemble condition with a temperature range from 300 K to 900 K and a pressure range from 0 Bar to 1000 Bar. More details about the DPGEN iterations can be found in Supporting Information or previous studies.[49,50]

Deep Potential Molecular Dynamics Simulations: Simulation details of large-size interfacial models were presented in Table S1 (Supporting Information). DeePMD simulations were conducted through the interface of DeePMD-kit[64–65] implemented in the LAMMPS package.[66] A three-dimensional periodic boundary condition was applied in all simulations. A time step of 1 fs was used to integrate equations of motion. First 2 ns NPT DeePMD simulations at room temperature were performed to observe interfacial structural evolutions and analyze formation of side products and the associated interfacial reconstruction. The pressures were set along the *x* and *y* directions as 1 bar. As for the *z* direction (vertical to the interface plane), a pressure of several tens to one hundred MPa was often applied to make heterogeneous interfaces in close contact in the experimental preparation process of ASSLBs. Thus the pressure was set along the *z* direction as 1000 Bar (100 MPa). Then the simulation time was extended to 10 ns to investigate Li-ion diffusion. The temperature was increased to 500 K to accelerate Li movement. Pressures in all three directions were set as 1 bar for the simulations of Li diffusion investigation, using the NPT ensemble condition.

Supporting Information

Supporting Information is available from the Wiley Online Library or from the author.

Acknowledgements

The authors gratefully acknowledge funding support from the Ministry of Science and Technology of the People's Republic of China (grant no. 2021YFB3800303), the National Natural Science Foundation of China (grant no. 52273223), DP Technology Corporation (grant no. 2021110016001141), the School of Materials Science and Engineering at Peking University, and the AI for Science Institute, Beijing (AISI). The computing resource of this work was provided by the Bohrium Cloud Platform (https://bohrium.dp.tech), which was supported by DP Technology.

Conflict of Interest

The authors declare no conflict of interest.

Data Availability Statement

The data that support the findings of this study are available from the corresponding author upon reasonable request.

Keywords

amorphous LiF coating, cathode-electrolyte interface, deep potential molecular dynamics, interfacial reconstructions, Li-ion diffusion

Received: February 19, 2024
Revised: April 8, 2024
Published online:

[1] X. Han, Y. Gong, K. K. Fu, X. He, G. T. Hitz, J. Dai, A. Pearse, B. Liu, H. Wang, G. Rubloff, Y. Mo, V. Thangadurai, E. D. Wachsman, L. Hu, *Nat. Mater.* **2017**, *16*, 572.
[2] Z. Zhang, Y. Shao, B. Lotsch, Y.-S. Hu, H. Li, J. Janek, L. F. Nazar, C.-W. Nan, J. Maier, M. Armand, L. Chen, *Energy Environ. Sci.* **2018**, *11*, 1945.
[3] A. Manthiram, X. Yu, S. Wang, *Nat. Rev. Mater.* **2017**, *2*, 16103.
[4] R. Schmuch, R. Wagner, G. Hörpel, T. Placke, M. Winter, *Nat. Energy* **2018**, *3*, 267.
[5] J. Janek, W. G. Zeier, *Nat. Energy* **2016**, *1*, 16141.
[6] F. Mizuno, A. Hayashi, K. Tadanaga, M. Tatsumisago, *Adv. Mater.* **2005**, *17*, 918.
[7] R. Murugan, V. Thangadurai, W. Weppner, *Angew. Chem., Int. Ed.* **2007**, *46*, 7778.
[8] Y. Seino, T. Ota, K. Takada, A. Hayashi, M. Tatsumisago, *Energy Environ. Sci.* **2014**, *7*, 627.
[9] Y. Kato, S. Hori, T. Saito, K. Suzuki, M. Hirayama, A. Mitsui, M. Yonemura, H. Iba, R. Kanno, *Nat. Energy* **2016**, *1*, 16030.
[10] N. Kamaya, K. Homma, Y. Yamakawa, M. Hirayama, R. Kanno, M. Yonemura, T. Kamiyama, Y. Kato, S. Hama, K. Kawamoto, A. Mitsui, *Nat. Mater.* **2011**, *10*, 682.
[11] Y. Wang, W. D. Richards, S. P. Ong, L. J. Miara, J. C. Kim, Y. Mo, G. Ceder, *Nat. Mater.* **2015**, *14*, 1026.
[12] Y. Inaguma, C. Liquan, M. Itoh, T. Nakamura, T. Uchida, H. Ikuta, M. Wakihara, *Solid State Commun.* **1993**, *86*, 689.
[13] L. Zhou, K.-H. Park, X. Sun, F. Lalère, T. Adermann, P. Hartmann, L. F. Nazar, *ACS Energy Lett.* **2019**, *4*, 265.
[14] L. Zhou, A. Assoud, Q. Zhang, X. Wu, L. F. Nazar, *J. Am. Chem. Soc.* **2019**, *141*, 19002.
[15] C. Wang, K. Fu, S. P. Kammampata, D. W. McOwen, A. J. Samson, L. Zhang, G. T. Hitz, A. M. Nolan, E. D. Wachsman, Y. Mo, V. Thangadurai, L. Hu, *Chem. Rev.* **2020**, *120*, 4257.
[16] R. Chen, Q. Li, X. Yu, L. Chen, H. Li, *Chem. Rev.* **2020**, *120*, 6820.
[17] C. Wang, J. Liang, Y. Zhao, M. Zheng, X. Li, X. Sun, *Energy Environ. Sci.* **2021**, *14*, 2577.
[18] A. Banerjee, X. Wang, C. Fang, E. A. Wu, Y. S. Meng, *Chem. Rev.* **2020**, *120*, 6878.
[19] A. Hayashi, H. Muramatsu, T. Ohtomo, S. Hama, M. Tatsumisago, *J. Alloys Compd.* **2014**, *591*, 247.
[20] S. Ito, S. Fujiki, T. Yamada, Y. Aihara, Y. Park, T. Y. Kim, S.-W. Baek, J.-M. Lee, S. Doo, N. Machida, *J. Power Sources* **2014**, *248*, 943.
[21] A. Sakuda, A. Hayashi, M. Tatsumisago, *J. Power Sources* **2010**, *195*, 599.
[22] H. Visbal, Y. Aihara, S. Ito, T. Watanabe, Y. Park, S. Doo, *J. Power Sources* **2016**, *314*, 85.
[23] N. Machida, J. Kashiwagi, M. Naito, T. Shigematsu, *Solid State Ionics* **2012**, *225*, 354.
[24] S. Yubuchi, Y. Ito, T. Matsuyama, A. Hayashi, M. Tatsumisago, *Solid State Ionics* **2016**, *285*, 79.
[25] Y. Ito, Y. Sakurai, S. Yubuchi, A. Sakuda, A. Hayashi, M. Tatsumisago, *J. Electrochem. Soc.* **2015**, *162*, A1610.
[26] A. Sakuda, H. Kitaura, A. Hayashi, K. Tadanaga, M. Tatsumisago, *J. Power Sources* **2009**, *189*, 527.
[27] J. H. Woo, J. E. Trevey, A. S. Cavanagh, Y. S. Choi, S. C. Kim, S. M. George, K. H. Oh, S.-H. Lee, *J. Electrochem. Soc.* **2012**, *159*, A1120.
[28] H. Komatsu, S. Banerjee, M. L. Holekevi Chandrappa, J. Qi, B. Radhakrishnan, S. Kuwata, K. Sakamoto, S. P. Ong, *J. Phys. Chem. C* **2022**, *126*, 17482.

[29] H. Tang, Z. Deng, Z. Lin, Z. Wang, I.-H. Chu, C. Chen, Z. Zhu, C. Zheng, S. P. Ong, *Chem. Mater.* **2018**, *30*, 163.
[30] M. L. Holekevi Chandrappa, J. Qi, C. Chen, S. Banerjee, S. P. Ong, *J. Am. Chem. Soc.* **2022**, *144*, 18009.
[31] J. Haruyama, K. Sodeyama, Y. Tateyama, *ACS Appl. Mater. Interfaces* **2017**, *9*, 286.
[32] B. Gao, R. Jalem, Y. Ma, Y. Tateyama, *Chem. Mater.* **2020**, *32*, 85.
[33] J. Haruyama, K. Sodeyama, L. Han, K. Takada, Y. Tateyama, *Chem. Mater.* **2014**, *26*, 4248.
[34] J. D. Howard, G. Evmenenko, J. J. Kim, R. E. Warburton, S. Patel, T. T. Fister, D. B. Buchholz, J. Greeley, L. A. Curtiss, P. Fenter, *ACS Appl. Mater. Interfaces* **2022**, *14*, 7428.
[35] A. Banerjee, H. Tang, X. Wang, J.-H. Cheng, H. Nguyen, M. Zhang, D. H. S. Tan, T. A. Wynn, E. A. Wu, J.-M. Doux, T. Wu, L. Ma, G. E. Sterbinsky, M. S. D'Souza, S. P. Ong, Y. S. Meng, *ACS Appl. Mater. Interfaces* **2019**, *11*, 43138.
[36] T. Cheng, B. V. Merinov, S. Morozov, W. A. Goddard, *ACS Energy Lett.* **2017**, *2*, 1454.
[37] A. Golov, J. Carrasco, *ACS Appl. Mater. Interfaces* **2021**, *13*, 43734.
[38] S. Boulineau, J.-M. Tarascon, J.-B. Leriche, V. Viallet, *Solid State Ionics* **2013**, *242*, 45.
[39] S. Wenzel, S. J. Sedlmaier, C. Dietrich, W. G. Zeier, J. Janek, *Solid State Ionics* **2018**, *318*, 102.
[40] K. Liu, Q. Zhang, S. Dai, W. Li, X. Liu, F. Ding, J. Zhang, *ACS Appl. Mater. Interfaces* **2018**, *10*, 34153.
[41] J. Huang, K. Du, Z. Peng, Y. Cao, Z. Xue, J. Duan, F. Wang, Y. Liu, G. Hu, *ChemElectroChem* **2019**, *6*, 5428.
[42] Z. Du, W. Peng, Z. Wang, H. Guo, Q. Hu, X. Li, *Ionics* **2018**, *24*, 3717.
[43] X. Xiong, Z. Wang, X. Yin, H. Guo, X. Li, *Mater. Lett.* **2013**, *110*, 4.
[44] X. Shi, Y. Pang, B. Wang, H. Sun, X. Wang, Y. Li, J. Yang, H. W. Li, S. Zheng, *Mater. Today Nano* **2020**, *10*, 100079.
[45] T. Zhao, L. Li, R. Chen, H. Wu, X. Zhang, S. Chen, M. Xie, F. Wu, J. Lu, K. Amine, *Nano Energy* **2015**, *15*, 164.
[46] S. Wang, A. Dai, Y. Cao, H. Yang, A. Khalil, J. Lu, H. Li, X. Ai, *J. Mater. Chem. A* **2021**, *9*, 11623.
[47] H.-J. Guo, H.-X. Wang, Y.-J. Guo, G.-X. Liu, J. Wan, Y.-X. Song, X.-A. Yang, F.-F. Jia, F.-Y. Wang, Y.-G. Guo, R. Wen, L.-J. Wan, *J. Am. Chem. Soc.* **2020**, *142*, 20752.
[48] J.-Y. Liang, X.-D. Zhang, Y. Zhang, L.-B. Huang, M. Yan, Z.-Z. Shen, R. Wen, J. Tang, F. Wang, J.-L. Shi, L.-J. Wan, Y.-G. Guo, *J. Am. Chem. Soc.* **2021**, *143*, 16768.
[49] T. Hu, F.-z. Dai, G. Zhou, X. Wang, S. Xu, *J. Phys. Chem. Lett.* **2023**, *14*, 3677.
[50] T. Hu, J. Tian, F. Dai, X. Wang, R. Wen, S. Xu, *J. Am. Chem. Soc.* **2023**, *145*, 1327.
[51] F. Fu, X. Wang, L. Zhang, Y. Yang, J. Chen, B. Xu, C. Ouyang, S. Xu, F.-Z. Dai, W. E., *Adv. Funct. Mater.* **2023**, *33*, 2303936.
[52] J. G. Kirkwood, *Chem. Rev.* **1936**, *19*, 275.
[53] J. G. Kirkwood, *J. Chem. Phys.* **1935**, *3*, 300.
[54] P.-Y. Yang, C.-W. Pao, *ACS Appl. Mater. Interfaces* **2021**, *13*, 5017.
[55] X. He, Y. Zhu, A. Epstein, Y. Mo, *npj Comput. Mater.* **2018**, *4*, 18.
[56] G. Kresse, J. Furthmüller, *Phys. Rev. B* **1996**, *54*, 11169.
[57] G. Kresse, J. Furthmüller, *Comput. Mater. Sci.* **1996**, *6*, 15.
[58] P. E. Blöchl, *Phys. Rev. B* **1994**, *50*, 17953.
[59] S. Grimme, *J. Comput. Chem.* **2006**, *27*, 1787.
[60] V. I. Anisimov, J. Zaanen, O. K. Andersen, *Phys. Rev. B* **1991**, *44*, 943.
[61] F. Zhou, M. Cococcioni, C. A. Marianetti, D. Morgan, G. Ceder, *Phys. Rev. B* **2004**, *70*, 235121.
[62] L. Zhang, J. Han, H. Wang, R. Car, W. E., *Phys. Rev. Lett.* **2018**, *120*, 143001.
[63] Y. Zhang, H. Wang, W. Chen, J. Zeng, L. Zhang, H. Wang, W. E., *Comput. Phys. Commun.* **2020**, *253*, 107206.
[64] H. Wang, L. Zhang, J. Han, W. E., *Comput. Phys. Commun.* **2018**, *228*, 178.
[65] J. Zeng, D. Zhang, D. Lu, P. Mo, Z. Li, Y. Chen, M. Rynik, L. Huang, Z. Li, S. Shi, Y. Wang, H. Ye, P. Tuo, J. Yang, Y. Ding, Y. Li, D. Tisi, Q. Zeng, H. Bao, Y. Xia, J. Huang, K. Muraoka, Y. Wang, J. Chang, F. Yuan, S. L. Bore, C. Cai, Y. Lin, B. Wang, J. Xu, et al., *J. Chem. Phys.* **2023**, 159.
[66] S. Plimpton, *J. Comput. Phys.* **1995**, *117*, 1.